On the Origins of Entanglement Constraints

D. Richter*

Institut für Festkörperforschung, Forschungszentrum Jülich, 5170 Jülich, Germany

B. Farago

Institut Laue-Langevin, 38042 Grenoble, France

R. Butera,† L. J. Fetters, and J. S. Huang

Corporate Research Laboratories, Exxon Research and Engineering Company, Annandale, New Jersey 08801

B. Ewen

Max-Planck-Institut für Polymerforschung, 6500 Mainz, Germany

Received September 24, 1992; Revised Manuscript Received November 10, 1992

ABSTRACT: We have studied the dynamic structure factors of poly(ethylene–propylene) alternating copolymer (PEP) and saturated polybutadiene (PEB-2). To investigate different models of entanglement formation, we varied the polymer volume fraction (PEB-2) and temperature (PEB-2 and PEP) and, thereby, systematically changed the two length scales considered to be important for the buildup of entanglements: namely, the contour length density and the random walk step length. In the framework of the scaling ansatz, our result is in the range of the binary contact models and excludes the packing model. Quantitatively, however, the scaling ansatz is not confirmed. Also, qualitative agreement is found with respect to the topological calculations by Iwata and Edwards. Our results are at variance with one of the basic relations of the Doi–Edwards theory of viscoelasticity, which relates the elastic response of a polymer melt with molecular chain parameters and the entanglement distance.

1. Introduction

In the plateau regime of the dynamic shear modulus a dense polymer system responds elastically like a rubber. This behavior has been ascribed to the existence of a temporary network built up by the mutually interpenetrating long-chain molecules. The role of the cross-links, thereby, falls to long-lived topological constraints or entanglements.[1,2] As for a rubber, the elasticity then arises from the entropy elasticity of the strands between the entanglements. The molecular origin of entanglements is not well understood, but current thinking postulates them to originate mainly from the topological nature of long-chain molecules as being flexible, nearly one-dimensional uncrossable objects. The occurrence of entanglements then is governed by two length parameters, the step length of the Gaussian random walk of the chains and the lateral distance between chains determining the amount of chain contour length per volume.[3-9]

In the reptation model,[10,11] up to now the most complete theory of the viscoelasticity of dense polymer systems, the topological constraints are modeled by a tube surrounding the coarse-grained chain profile. Polymer motions are restricted to the interior of the tube which after a terminal time is left by creep motion through its ends. The tube diameter d may be identified with the distance between entanglements. The Doi–Edwards theory of viscoelasticity,[11] which is based on the reptation model, relates the plateau modulus, a property accessible to rheological measurements, to the microscopic tube diameter of the reptation model.[12]

$$G_N^\circ = \frac{4}{5}\frac{\langle R_e^2\rangle}{M}\frac{\rho k_B T}{d^2} \tag{1}$$

where $\langle R_e^2\rangle = nNC_\infty l_0^2$ is the mean square end-to-end distance, C_∞ the characteristic ratio, l_0 the average main-chain bond length, n the average number of bonds per monomer, M the molecular weight, N the degree of polymerization, and ρ the polymer density. Equation 1 is one of the fundamental relationships of the Doi–Edwards theory relating macroscopic viscoelastic properties to the microscopic chain confinement.

Until recently, the microscopic picture of a network of entanglements or a tube confining the polymer motion has been mainly inferred from rheometry,[1] revealing the viscosity and the plateau modulus G_N°, and from the anomalous diffusion behavior of long-chain molecules.[13] In 1990, applying neutron spin–echo (NSE) spectroscopy, Richter et al.[14] reported a first direct microscopic observation of the entanglement distance d, which in NSE experiments reveals itself as an intermediate dynamic length beyond which the relaxation of density fluctuations is strongly impeded.

In a recent paper[15] we gave a detailed account of these NSE experiments and their interpretation. Here we present a study aimed at the origin of entanglement constraints. We report NSE experiments on the temperature dependence of the dynamic structure factors of saturated polybutadiene (PEB-2) and poly(ethylene–propylene) alternating copolymer (PEP). For PEB-2 we

* To whom correspondence should be addressed.
† Present address: du Pont Marshall Laboratory, 3500 Grays Ferry Ave., Philadelphia, PA 19146.

0024-9297/93/2226-0795$04.00/0

also varied the polymer volume fraction. The experiments were supplemented by temperature-dependent viscoelastic and small-angle neutron scattering (SANS) investigations of PEP aimed at the plateau modulus and the Kuhn length $l_K = l_0 C_\infty$ (l_0 = bond length). With this experimental approach we systematically changed the parameters which are supposed to determine the entanglement formation. In varying the polymer volume fraction, we studied the dependence of d on the contour length density; in changing the temperature and thereby the Kuhn length, we investigated the effect of the random walk step length l_K.

In section 2 we outline different ideas on the molecular origin of entanglements. Two classes of models are discussed: (i) the scaling models try to understand the important features of entanglement formation in terms of dimensional analysis and scaling ideas. Since two independent length scales appear to be involved, a large variety of scaling models are possible. We present a general scaling model,[3] the packing model,[4] and two binary contact models.[5-7] The second class envelops topological approaches where in terms of mathematical models entanglement constraints are calculated.[8,9] Section 3 describes the experimental procedures, including sample preparation and characterization, neutron spin–echo experiments, and rheological experiments. Section 4 presents our results on the two polymers, PEB-2 and PEP. NSE data on polymer melts for different temperatures (PEP, PEB-2) and in concentrated solution for different polymer volume fractions (PEB-2) are displayed. Furthermore, temperature-dependent viscoelastic data on PEP are shown. In section 5 we discuss the experimental results. The different models for entanglement formation are scrutinized in the light of the experimental temperature and density dependence of the entanglement distance. Relating the temperature dependence of the plateau modulus, the microscopic entanglement distance, the chain flexibility, and the density, we investigate the relation between plateau modulus and tube diameter as predicted by the reptation model of viscoelasticity.[11] Section 6 summarizes our work.

2. Models for Entanglement Formation

The interpretation of viscoelastic properties of dense long-chain polymers is based on the existence of an intermediate dynamic length scale—the entanglement length—which in analogy to rubber-elasticity acts like the mesh of a temporary network. In the reptation theory[11,12] this length becomes the tube diameter, signifying the lateral constraints for polymer motion. Though the entanglement distance is of crucial importance of our understanding of viscoelasticity in polymers, its molecular origin is still not very well known. Different ideas have been brought forward in order to draw a microscopic or molecular picture of the entanglement phenomenon: Based on the concept of a dominating influence of chain contour length density, Graessley and Edwards proposed a general scaling ansatz;[3] de Gennes and others[6,7] promoted the idea of the amount of interchain contacts being the essential feature; and Ronca,[16] Lin,[17] and Kavassalis and Noolandi[4] proposed a packing criterion for entanglement formation. Partially related to the interchain contact approach but conceptually different is the topological model by Edwards[8] and Iwata and Edwards,[9] who treat the entanglement problem in terms of integral invariants. In the following we briefly outline the different concepts and work out the specific predictions on the dependence of the entanglement distance d on polymer density and segment length or characteristic ratio C_∞.

2.1. The Scaling Model. Graessley and Edwards[3] assumed that large-scale interactions in dense polymer systems should relate only to the chainlike structure of the molecules, the essential effect being the topological interaction arising from the mutual uncrossability of chains. The important quantity, therefore, is the chain contour length per unit volume (L/V). In polymer networks the modulus G/kT reflects the cross-link density. In terms of the rubber analogue the plateau modulus G_N° should relate to the interaction density and be largely determined by the contour length density. More bulky chains like polystyrene (PS) correspond to a lower contour length density exhibiting a smaller G_N°, while slim chains like polyethylene (PE) have a high contour length density and consequently a high plateau modulus. To construct scaling relations, dimensionless quantities are required. They may be obtained in considering the length characteristic for the polymer conformation, the Kuhn length $l_K = C_\infty l_0$. With the contour length density $L/V = \nu L$, where $\nu = N_a \rho\phi/M$ is the number of chains/volume (N_a = Avogadro's number, ϕ = monomer concentration, ρ = density) and $L = Ml_0/m_0$ (m_0 = molecular weight/bond), the scaling relation between the plateau modulus and the contour length density then reads

$$\frac{G_N^\circ l_K^3}{k_B T} = F(\nu L l_K^2) \tag{2}$$

Considering further $\nu L l_K^2 \sim \phi$ and the experimental relation $G_N^\circ \sim \phi^a$ (with a between 2 and 2.3), eq 2 assumes the form of a power law

$$\frac{G_N l_K^3}{k_B T} \sim (\nu L l_K^2)^a \tag{3}$$

using the relation of ν, l_K, and L to molecular quantities (see above) they arrive at

$$G_N^\circ \sim k_B T C_\infty^{2a-3} \left(\frac{\rho\phi}{m_0}\right)^a l_0^{3a-3} \tag{4}$$

Finally, with eq 1 for d we obtain

$$d^2 \sim C_\infty^{4-2a} \left(\frac{\rho\phi}{m_0}\right)^{1-a} l_0^{5-3a} \tag{5}$$

2.2. Packing Models. Packing models relate the occurrence of an entanglement to the gradual buildup of geometrical hindrances due to the presence of other chains. More precisely, entanglements are determined by a volume through which a certain number of other chains have to pass, or a mean number of neighboring chain segments belonging to other noninterrupted chains (chain ends do not count) is required to restrict the lateral degree of freedom. This approach is based on the observation that for many polymers the product of the density of entanglement strands $n_\nu = \rho N_a/M_e$, where $M_e = N_e m_0$ is the entanglement molecular weight, and the volume spanned by the entanglement distance is roughly constant[16,17]

$$n_t = \text{const} = n_\nu d^3 = \frac{\rho N_a}{M_e}\left(C_\infty \frac{M_e}{m_0} l_0^2\right)^{3/2} \tag{6}$$

Kavassalis and Noolandi[4] have extended the theory and take explicitly into account the effect of chain ends, which adds a factor $(1 - M_e/M)$ to eq 6. The modified theory describes the transition from entangled to nonentangled behavior at M_e in terms of a mean field second-order phase transition. In replacing ρ by $(\rho\phi)$ in eq 6, the theory may also be extended to concentrated solutions. Neglecting

the influence of chain ends, eq 6 yields for the entanglement distance ($d^2 = C_\infty l_0^2 N_e$)

$$d^2 \approx \frac{1}{(\rho\phi/m_0)^2 C_\infty^2 l_0^4} \tag{7}$$

We note that as a consequence of the packing criterion, the entanglement distance increases with increasing tendency of a chain to coil—coiling diminishes the presence of other coils and the entanglement volume increases. Furthermore, as a result of packing, the length of an entanglement strand $N_e \sim d^2$ is inversely proportional to the bond density. Packing is a special case of general scaling for $a = 3$.

2.3. Binary Contact Model. A longstanding alternative scaling approach designed to grasp the nature of an entanglement is that, where an entanglement is defined by a certain fixed number of binary contacts along the chain.[6,7] This argument again is of a topological nature dwelling on the noncrossability of polymer chains. Let $\varphi = N_a\rho\phi/(m_0 C_\infty)$ be the density of Kuhn segments; then the number of n_b of binary contacts/volume is given by

$$n_b \sim \varphi^2 l_K^3 \tag{8}$$

For the number entanglement strands n_e/volume we have

$$n_e = \frac{(\phi\rho)N_a}{M_e} = \frac{(\phi\rho)N_a}{N_e m_0} \tag{9}$$

The desired number of binary contacts per entanglement strands is then

$$\frac{n_b}{n_e} = \text{const} \sim \left(\frac{\rho\phi}{m_0}\right) l_0^3 C_\infty N_e \tag{10}$$

Using eq 1 for the entanglement distance

$$d^2 \sim \frac{1}{(\rho\phi/m_0) l_0} \tag{11}$$

is obtained (general scaling $a = 2$).

Recently, Colby and Rubinstein[18] proposed an alteration of this scaling ansatz, conjecturing that an entanglement was determined by a constant number of binary contacts in the entanglement volume d^3, bringing thus together packing and contact models. The scaling relation for the entanglement distance then reads ($a = {}^7/_3$)

$$d^2 \sim \frac{1}{C_\infty^{2/3} l_0^2 (\rho\phi/m_0)^{4/3}} \tag{12}$$

We further would like to note that the apparent inability of simple scaling to give a definite answer relates to the fact that the entanglement problem considered as a geometrical phenomenon contains two independent length scales—the step length of the random walk l_K and the interchain distances given by the contour length density $(L/V)^{-1/2}$. Therefore, besides scaling arguments, further assumptions as explained above are necessary.

2.4. The Topological Approach. Like the scaling approach, the toplogical calculations are based on the assumption that the entanglement problem may be purely geometrical, i.e., a mathematical problem, where dynamic effects do not play a role. The topological calculations go beyond scaling in that the topological invariants of the geometrical constraints are calculated rather than conjectured as in the scaling arguments. As entanglements are considered to be a purely geometrical effect, the entanglement distance can only be a function of the two length scales in the problem—the step length of the random walk of the chains l_K and the distance between chain contours $(L/V)^{-1/2}$. Using the Gaussian topological invariant, which counts the windings swept out by one curve around another, Edwards[8] calculated the dependence of the tube diameter on the chain contour density for two limiting cases. For pure random flight polymers

$$d \sim \frac{1}{l_K(L/V)} \sim \frac{1}{(\rho\phi l_0/m_0) l_K} \tag{13}$$

is obtained. This result agrees with a scaling argument given earlier by Doi[19] and corresponds to the Graessley–Edwards scaling formula for $a = 3$ which is also followed by the packing models.

The other limiting case concerns locally smooth chains. For the case of a Gaussian chain in a network of rods, Edwards found $d \sim (L/V)^{-1/2}$, which agrees with the above-discussed binary contact model. Finally, considering wormlike chain bridges, the differences in the power laws between the two limiting cases and exponents between -1 and $-{}^1/_2$ may be obtained.

Recently, Iwata and Edwards[9] extended the Gaussian integral method to so-called localized Gaussian integrals. In this approach the chain is subdivided consistently into so-called local chains. Their interaction can be treated in terms of two-body invariants like the Gaussian integral while the multibody encounters of the full chains cannot be easily identified by this method. These calculations are the most advanced in relating chain properties to topological hindrance. The theory introduces a new quantity, the topological interaction parameter $\bar{\gamma}$, which measures the capability of a chain to entangle and may be considered as a property individual to each chain as the characteristic ratio. $\bar{\gamma}$ is mainly determined by the diameter of a polymer chain. As one would have expected, polymers entangle more if the chain diameter is small or the contour length density is high. Furthermore, $\bar{\gamma}$ appears to be also related to the size of C_∞—the larger C_∞ becomes, the more a chain reaches out in space and the better it entangles. An analytic functional dependence, however, cannot be read off from their results. Finally, for the concentration dependence of the plateau modulus they calculate $G_N \sim \phi^a$, where a increases with decreasing concentration ($1.97 \le a \le 2.2$). For high concentrations their result agrees with $d \sim (\rho\phi/m_0)^{-1/2}$.

Besides this mathematical approach, there are also more heuristic topological considerations under discussion. A typical model of this class is by Wu,[20] who considered entanglements as knots or hooks between chains. Here, it is believed that with increasing chain flexibility the chains will be able to form hooks more easily. If $n_h = 1/(C_\infty l_0)$ is the number of node points per length along the chain, then the probability of a hook between chains is proportional to n_h^2 (two chains have to have a node at the same position). Therefore, the arc length between two entanglements should be $L_e^2 \sim 1/n_h^2$. With that we arrive at $N_e \sim C_\infty^2$ or

$$d^2 \sim C_\infty^3 \tag{14}$$

We consider this ansatz as inadequate since it neglects completely the effect of contour length density. Nevertheless, comparing data for different polymers, Aharoni[21] has deduced a correlation of the form $N_e \sim C_\infty^2$, a result contrary to Lin's analysis.

3. Experimental Section

3.1. Sample Preparation and Characterization. The polyisoprenes and polybutadienes were prepared via standard anionic polymerization techniques: *tert*-butyllithium, purified by sublimation, was the initiator. The deuterated monomers

Table I
Polymer Molecular Characteristics

sample	$M_w \times 10^{-4}$ [a]	M_z/M_w [b]	M_w/M_n [b]
PEP-d_{10}	8.38	1.03	1.05
PEP-h_{10}	8.22	1.02	1.05
PEP-h_{10} III	36.70	1.03	1.04
PEP-2-h_8	7.05	1.04	1.04
PEB-2-d_8	7.32	1.02	1.04

[a] Light scattering. [b] Size exclusion chromatography.

were obtained from Cambridge Isotopes. The microstructure (H- or D-NMR) of the polyisoprenes was 75% cis-1,4, ~18% trans-1,4, and ~7% 3,4 while that of the polybutadienes was ~40% cis-1,4, ~53% trans-1,4, and ~7% 1,2. Size exclusion chromatography was used to evaluate the heterogeneity indices.

The saturation by hydrogen or deuterium of the polydienes was done by using palladium on calcium carbonate. The procedure followed that of Rachapudy et al.[22] NMR analysis showed that saturation levels of >99.7% were obtained. The saturation of polyisoprene yielded essentially alternating amorphous poly(ethylene–propylene) (PEP), while polybutadiene yielded the crystalline poly(ethylene–1-butene) copolymer which is designated as PEB-2 (where the integer denotes the approximate number of ethyl branches per 100 backbone carbons). Densities at 23.1 °C for the amorphous polymers were measured in a density gradient column. Weight-average molecular weights were evaluated via a Chromatix KMX-6 low-angle laser photometer. For the case of the PEB-2 materials, the molecular weights of the parent polybutadienes were measured and corrected for saturation. The sample characteristics are given in Table I.

3.2. Neutron Scattering. All neutron scattering experiments to be discussed in the following were carried out with the aid of neutron spin–echo spectroscopy.[23] In such an experiment, the neutron polarization P is measured as a function of the applied guide field H for various scattering angles (ϑ). For a coherently scattering specimen, $P(Q,H)$ directly gives the normalized scattering function $S(Q,t)/S(Q,0)$, where $Q = (4\pi/\lambda)\sin\vartheta$ is the momentum transfer, λ the neutron wavelength, and t the time, which is proportional to H and λ^3. The scattering contrast generally arises from the differences in scattering length of the deuterated matrix or the deuterated solvent and a protonated polymer. Under these conditions the coherent scattering of the individual chain or its pair correlation function is measured.

We used sealed Nb containers which were loaded under inert conditions to avoid oxygen which could degrade the polymers at high temperatures. The samples were heated in a vacuum furnace up to 600 K with a temperature stability of $\Delta T = \pm 1$ °C. The backgrounds from the matrices—nearly entirely inelastic scattering—and from the container were measured separately and substracted using the proper transmission factors. Resolution corrections were performed using the instrumental resolution function obtained from a glassy PS standard (90/10 d/h) at room temperature.

3.3. Rheological Measurements. Rheological measurements were performed on a high molecular weight PEP sample (PEP III) (see Table I) using a Rheometrics System 4 rheometer with 25-mm-diameter plates in the oscillatory shear mode, with gap spacings which ranged between 1 and 2 mm. The sample was surrounded by a nitrogen atmosphere during all measurements. Isothermal frequency scans were performed using frequencies between 10^{-3} and 100 rad/s. The strain amplitude was kept as small as possible, but ranged between $\gamma = 0.02$ and $\gamma = 0.5$, depending upon the frequency and temperature being used. Linearity of response was checked whenever the strain was increased, and all data reported are within the linear regime. Adjustments were made during each temperature change to account for thermal expansion of the plates and sample.

The sample preparation and loading procedure were as follows: First the sample was dried to constant weight under vacuum at 75 °C, producing a smooth bubble-free sample. Approximately 1.1 g of this material was compression molded between mylar sheets at 70 °C for 23 min. The mold was then cooled to room temperature under a slight pressure. The sample was released from the mold, placed on the lower plate, and squeezed between the plates until a slight normal force was registered. The temperature was raised to 100 °C and held there for 20 min. While at 100 °C the sample was squeezed until it began to flow. It was then trimmed and raised to 150 °C for approximately 1 h to allow complete adhesion to the plates. The temperature was then decreased to 60 °C, the sample was trimmed, and the temperature was raised again to 150 °C; the sample was held at that temperature for 30 min before starting the measurements.

4. Results

To pursue the problem of entanglement formation, a series of NSE experiments were performed on PEB-2 where the polymer volume fraction and temperature were changed. These experiments were supplemented by a temperature-dependent study of PEP, where we also investigated the plateau modulus. PEB-2 (essentially PE with one ethyl branch every 50 main-chain bonds) combines a very fast Rouse relaxation with strong topological constraints[15] and is therefore very well suited for a NSE study, which is always limited by spectral resolution. For PEB-2 it was possible to access a large concentration and temperature range using neutrons of short wavelength ($\lambda = 8.5$ Å) covering a time window $0.3 \le t \le 17$ ns. At this wavelength the intensity is about 4 times higher than that at $\lambda \approx 11$ Å, which was used in earlier NSE studies on melt dynamics.[14,15,24,25]

For the dilution experiments we used the oligomer $C_{19}D_{40}$, which can be considered as athermal. The deuterated paraffin was obtained from Cambridge Isotopes and was 98% deuterated as verified by proton NMR. The diluted samples were produced in diluting a master alloy of 90/10 d/h PEB-2 with the oligomer. To attempt a proper background correction, we measured the scattering from 100% deuterated PEB-2 and a pure $C_{19}D_{40}$ sample. The background turned out to be purely inelastic and increasing with temperature. The subtraction was performed in combining respective proportions of the scattering from these two samples. To estimate whether the paraffin causes any SANS when contrasted with the protonated PEB-2 fraction in the mixed samples, we estimated its scattering contribution from an RPA formula for a three-component mixture, neglecting any specific interaction effects.[26] In the worst case at 75% dilution and at $Q = 0.15$ Å^{-1}, the SANS contribution from the paraffin scattering is estimated to be below 3% of the total signal, rendering it negligible.

Experiments were performed in the concentration range $0.25 \le \phi \le 1$ polymer volume fraction at $T = 509$ K. Temperature-dependent measurements were carried out at $\phi = 1$ and $\phi = 0.5$ covering a temperature range $418 \le T \le 556$ K. At each concentration and temperature, spectra of at least three different Q values were recorded. Thereby, depending on temperature and concentration, a Q range $0.052 \le Q \le 0.155$ Å^{-1} was covered.

Figure 1 presents representative spectra at three different polymer volume fractions. To directly visualize the effect of entanglement constraints the data are plotted against the dimensionless scaling variable $u = Q^2l^2(Wt)^{1/2}$ of the Rouse model,[27,28] where l is the segment length, $W = 3kT/(\zeta l^2)$ (ζ = segmental friction coefficient), and t is the time. In such a presentation the dynamic structure factor originating from Rouse motion collapses to a master curve.[15,28,29] The Q-dependent splitting arises from the existence of the entanglement length at an intermediate dynamic length scale and thus demonstrates the presence of entanglement constraints.[14,15]

The solid lines present the effective medium model by Ronca.[16] This model describes the dynamic structure factor in the crossover regime from unrestricted Rouse

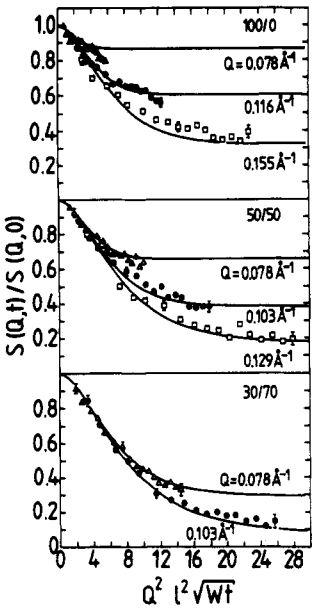

Figure 1. NSE spectra obtained from PEB-2 at 509 K for three different volume fractions in a Rouse scaling presentation: upper part $\phi = 1$; middle part $\phi = 0.5$; lower part $\phi = 0.3$. The solid lines are the results of fits with the Ronca model.[16]

motion to entanglement-controlled behavior and contains two parameters: the tube diameter or entanglement distance d and the "Rouse rate" Wl^4. Thereby, the plateaus developing at large u signify the amount of constraints—a high plateau value translates into a small entanglement distance and vice versa. Comparing spectra at similar Q values and different polymer concentrations, we observe a drastic decrease of the constraints: e.g., at $\phi = 1.0$ the plateau for $Q = 0.116$ Å^{-1} extrapolates to about 0.6; at $\phi = 0.5$ the plateau for $Q = 0.103$ Å^{-1} reaches already below 0.4, while at $\phi = 0.3$ this level has dropped to less than 0.1. We also note that even at a polymer volume fraction of only 0.3 we still find pronounced deviations from scaling with the Rouse variable. Thus even at this concentration a well-defined intermediate dynamic length scale arising from the entanglement constraints can be observed.

As has been discussed earlier[15] and may also be seen from the upper set of spectra in Figure 1 for the PEB-2 melt, the Ronca model and the experimental results show some disagreement. Similar deviations occur for the other samples with high polymer volume fraction ($\phi \geq 0.7$), while they are absent for the two lower concentrations displayed. In the earlier study[15] we have also shown that applying the local reptation model of de Gennes,[30] which considers the equilibration of density fluctuations along the fixed tube, a better agreement between experiment and theory may be achieved. The local reptation model gives an explicit expression for $S(Q,t)$ to first order in $(Qd)^2$

$$S(Q,t)/S(Q,0) = 1 - \frac{Q^2d^2}{36} + \frac{Q^2d^2}{36}\exp\left(\frac{u^2}{36}\right)\mathrm{erfc}\left(\frac{u}{6}\right) \quad (15)$$

thereby, $u = Q^2l^2(Wt)^{1/2}$ is the Rouse variable defined above. Since the local reptation model neglects the short-time unrestricted Rouse motion, this must be excluded in the analysis with eq 15. Consequently, the value of the Rouse rate Wl^4 entering into $u = Q^2l^2(Wt)^{1/2}$ is determined from the short-time part of the spectra. Figure 2 presents Rouse scaling plots of the initial part of the spectra for the same concentrations as shown in Figure 1. The solid line depicts the Rouse dynamic structure factor serving as a master curve. From fits of these data involving always only the Rouse rates as a fit parameter, the related monomeric friction coefficients ζ were obtained. For the

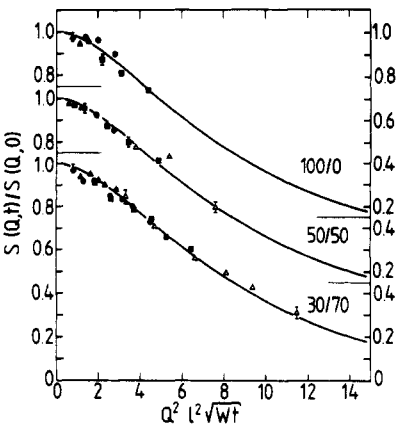

Figure 2. Initial decrease of the dynamic structure factors from PEB-2 at volume fractions $\phi = 1$, $\phi = 0.5$, and $\phi = 0.3$ in a Rouse scaling presentation. The solid lines represent the Rouse master function. The data points from the upper curve represent the Q values: 0.078, 0.116, and 0.155 Å^{-1}; from the middle curve: 0.052, 0.078, 0.116, and 0.155 Å^{-1}; from the lower curve: 0.052, 0.065, 0.078, and 0.116 Å^{-1}.

Table II
Friction Coefficients and Entanglement Distances in Concentrated PEB-2 Solutions and Melts at $T = 509$ K

polym vol frac φ	Wl^4 (10^{-13} Å^4 s^{-1})	ζ [10^{-10} (dyn cm) s^{-1}]	d (Å) de Gennes	d (Å) Ronca
1.00	7.0 ± 0.7	4.0 ± 0.4	43.5 ± 0.7	42.8 ± 0.9
0.90	9.2 ± 0.8	3.0 ± 0.3	48.0 ± 0.5	45.5 ● 0.7
0.70	14.3 ± 1.5	1.9 ± 0.2	55.1 ● 0.4	52.8 ● 0.6
0.60	11.7 ± 0.8	2.3 ± 0.2	59.9 ● 0.7	58.9 ± 1.3
0.50	18.2 ± 1.1	1.5 ± 0.1	67.0 ± 0.6	62.0 ● 0.7
0.35	29.8 ± 1.1	0.92 ± 0.03	83.6 ± 0.3	77.5 ● 1.4
0.30	33.7 ± 1.2	0.82 ± 0.03	102.6 ● 1.8	88.4 ± 1.5
0.25	37.2 ● 1.5	0.74 ± 0.03	- -	- -

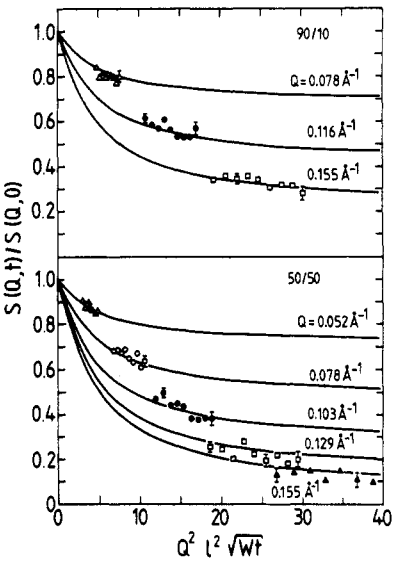

Figure 3. Rouse scaling representation of the long-time tails of the PEB-2 spectra at $\phi = 0.9$ and $\phi = 0.5$. The solid lines are fits with the local reptation model.[30]

determination of ζ from $Wl^4 = 3kTl^2/\zeta$ we assumed $l^2 = C_\infty l_0^2 = 13.05$ Å^2 [31] (Table II).

Keeping these Rouse rates fixed, the long-time tails ($t \geq 7$ ns)[15] of the spectra were then fitted with the dynamic structure factor of local reptation (eq 15). Figure 3 displays the results for $\phi = 0.9$ and $\phi = 0.5$. Apparently, the local reptation model fits the spectra significantly better than the Ronca model. In particular, it accounts for the continuous, gradual decay of $S(Q,t)/S(Q,0)$ even at large u. Because of the better accuracy of the de Gennes local

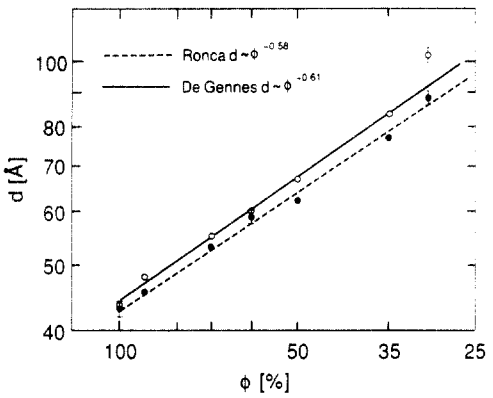

Figure 4. Double logarithmic presentation of the entanglement distance or tube diameter d for PEB-2 at 509 K as a function of polymer volume fraction ϕ: (○, solid line) results from a fit with local reptation; (●, dashed line) fit with the Ronca model.

reptation model, all entanglement distances were evaluated in terms of this model—the values for d from both models differ only slightly, the maximum discrepancy occurring at the lowest polymer concentration. We would like to note that at low polymer volume fraction the crossover from unrestricted Rouse motion to local reptation shifts toward the outer part of the experimental time window, adding some uncertainty to the evaluated results. Therefore we also fitted all data sets in terms of the Ronca model, where all data points were considered.

Figure 4 displays the results for d as a function of ϕ (see also Table II). The open symbols represent the outcome of the fit with eq 15 while the full circles are the Ronca results. The entanglement distances from the Ronca fit come out slightly smaller—on the average by about 5%—than those obtained from local reptation. Within experimental accuracy, however, the dependence on ϕ is identical. The solid line $d \sim \phi^{-0.61\pm0.02}$ corresponds to local reptation while the dashed line $d \sim \phi^{-0.58\pm0.02}$ represents the Ronca results. At $\phi = 0.3$ in the case of local reptation the d value is definitely larger than suggested by the power law (solid line). The results from the Ronca treatment point in the same direction though the deviation is not as large. For $\phi = 0.25$ the Q-dependent splitting in the scaling representation of the data points is absent, and consequently an entanglement distance cannot be determined anymore with certainty. The observed deviation from the power law behavior at low ϕ may result from the crossover to the semidilute regime, where a larger exponent ($-3/4$) is expected. This is further underlined by our failure to observe clear indications of constraints at $\phi = 0.25$, implying that there the tube diameter must be considerably larger than what would be extrapolated from the high-concentration range.

We also addressed the temperature dependence of the microscopic dynamics of PEB-2. Figure 5 presents NSE spectra taken from the melt ($\phi = 1$) at 418 and 483 K. Comparing the spectra qualitatively, we observe a strong increase in initial relaxation—the spectra at 483 K drop much faster than those at 418 K while the values reached at long times differ only slightly. Obviously the topological constraints change only slightly. This is reflected in the experimental result for the temperature-dependent entanglement distance displayed in Figure 6 (see also Tables III and IV). Again the data points were obtained by the two-step evaluation procedure involving short-time Rouse and long-time de Gennes model fits. (For comparison in Table III we also display the corresponding results from a fit with the Ronca model. Within experimental error they agree with the result of the local reptation model.)

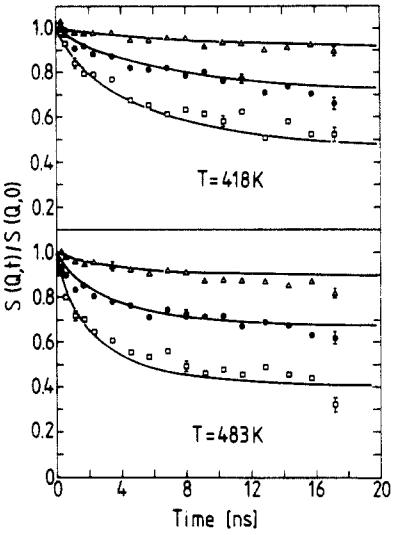

Figure 5. NSE spectra from PEB-2 for two different temperatures. The solid lines are results of a fit with the Ronca model: (△) $Q = 0.077$ Å^{-1}; (●) $Q = 0.116$ Å^{-1}; (□) $Q = 0.155$ Å^{-1}.

The results obtained for $\phi = 1.0$ and $\phi = 0.5$ are displayed in Figure 6. They are compatible with an identical temperature coefficient for both concentrations. The broken line represents the best fit for the $\phi = 1$ data

$$d = 23.5 \exp((1.2 \pm 0.2) \times 10^{-3} T) \qquad (16)$$

Finally, the temperature-dependent Rouse rates or the monomeric friction coefficients respectively were evaluated in terms of WLF shift factors $\log a_T = c_0(T - T_0)/(T - T_\infty)$. Within experimental accuracy, the WLF relation based on the viscosity results from Carella et al.[32] ($T_\infty = 124$ K, $c_0 = 6.35$ for $T_0 = 270$ K) for their sample with the lowest methyl-branch content describes the temperature dependence of the microscopic Rouse rates.

We also investigated the temperature dependence of the dynamic structure factor from PEP. Using a wavelength of $\lambda = 11.25$ Å, which offers an experimental time window of $0.7 \le t \le 36$ ns, we recorded spectra at eight different temperatures over a temperature range $373 \le T \le 598$ K. At each temperature spectra at three different momentum transfers were measured ($Q = 0.068$, 0.097, 0.126 Å^{-1}). The spectra were fitted in terms of the Ronca model, which provided a good description of the experimental spectra.[33] Figure 7 displays selected spectra taken at $Q = 0.126$ Å^{-1} at different temperatures. The solid lines are the results of the respective Ronca fits which at each temperature were performed under the consideration of all three available Q values. The results are given in Table V. Again the spectra are characterized by two subsequent time regimes: an initial decay succeeded by a plateau region which becomes increasingly better separated with rising temperature. Higher temperature causes a strong acceleration of the initial relaxation and a decrease in the number of constraints—the plateau level appears to drop with increasing T. Only for the spectra at the two highest temperatures (548 and 598 K), no further change in the long-time plateau level occurs. Figure 8 displays the resulting temperature-dependent entanglement distance. This parameter increases with T ($d \ln d/dT \simeq 2.8 \times 10^{-3}$ K^{-1}) until leveling off above 500 K. We note that the temperature coefficient of d for PEP is much larger than that for PEB-2 ($K_{PEP} \approx 2.3 K_{PEB}$). Figure 8 also includes results on the temperature dependence of the mean square radius of gyration $\langle R_g^2 \rangle \sim C_\infty(T)$ from PEP obtained by SANS.[34] R_g^2 decreases with increasing temperature. Thereby, the temperature coefficient de-

Table III
Entanglement Distances, Rouse Rates, Characteristic Ratios, Densities, and Invariant of the Rubber Analogue for PEB-2

T (K)	Wl^4 (10^{-13} Å^4 s^{-1})	d (Å) de Gennes	d (Å) Ronca	C_∞[a]	ρ (g/cm^3)	$d^2G_N^\circ/\rho TC_\infty$
418	1.47 ± 0.2	38.5 ± 0.6	38.4 ± 1.2	6.52	0.783	1.53 ± 0.05
446	2.81 ± 0.4	39.8 ± 0.5	39.9 ± 0.7	6.32	0.767	1.61 ± 0.05
463	3.60 ± 0.5	42.2 ± 0.6	42.6 ± 1.0	6.19	0.757	1.81 ± 0.06
484	3.95 ± 0.4	40.9 ± 0.6	40.2 ± 0.7	6.05	0.746	1.68 ± 0.06
509	7.00 ± 0.7	43.5 ± 0.7	42.8 ± 0.9	5.87	0.733	1.97 ± 0.07
529	7.30 ± 0.7	44.1 ± 0.4	43.5 ± 0.6	5.74	0.722	1.95 ± 0.04
556	8.00 ± 0.5	45.8 ± 0.7	44.2 ± 0.7	5.57	0.708	2.10 ± 0.07

[a] C_∞ is based on the SANS results at 413 K for polyethylene and PEB-2. See ref 31; Liese, G.; Fischer, E. W.; Ibel, K. *J. Polym. Sci., Polym. Lett. Ed.* **1975**, *13*, 39; and Horten, J. C.; Squires, G. L.; Boothroyd, A. T.; Fetters, L. J.; Rennie, A. R.; Glinka, C. J.; Robinson, R. A. *Macromolecules* **1989**, *22*, 681. The combined data yields $R_G = 0.45M^{0.50}$, a value in excellent agreement with that from dilute solution measurements under Θ conditions.

Table IV
Entanglement Distances and Rouse Relaxation Rates for a $\phi = 0.5$ Concentrated Solution of PEB-2 in $C_{19}D_{40}$

T (K)	Wl^4 (10^{-13} Å^4 s^{-1})	d (Å)
463	11.0 ± 1.3	65.1 ± 0.8
509	18.2 ± 1.1	67.0 ± 0.8
556	25.5 ± 1.9	72.7 ± 1.1

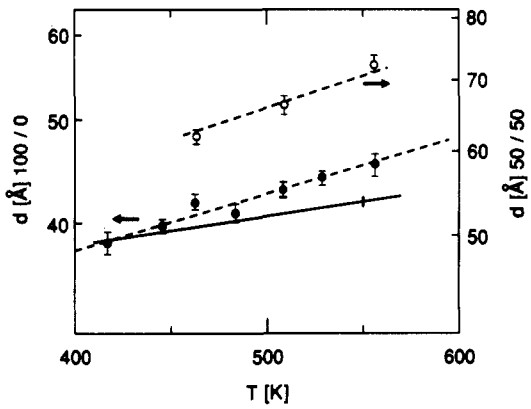

Figure 6. Temperature dependence of the entanglement distance d of PEB-2: (●) $\phi = 1$; (○) $\phi = 0.5$. The dashed lines are guides for the eye. The solid line gives the prediction of the general scaling model of Graessley and Edwards[3] (see text).

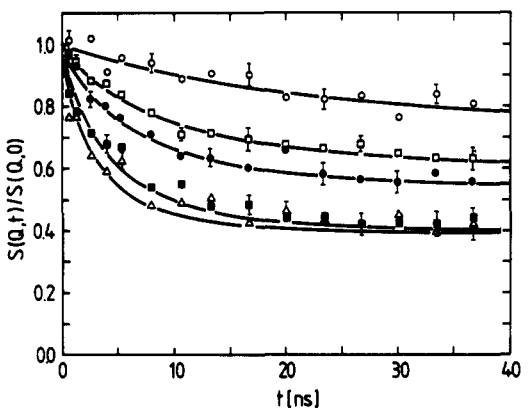

Figure 7. Experimental spectra from PEP at $Q = 0.126$ Å^{-1} at different temperatures: (○) 373 K; (□) 423 K; (●) 457 K; (■) 548 K; (△) 598 K. The solid lines correspond to fits with the Ronca model (see text).

creases with increasing T. It thus has the opposite temperature behavior as d. Finally, Figure 9 presents the temperature shift factor of the Rouse relaxation rates $a_T = ([\zeta l^2]_{T_0}/[\zeta l^2]_T)(T/T_0)$ taken from the measured relaxation rates $Wl^4 = 3kTl^2/\zeta$ and using $l^2 = C_\infty(T)l_0^2$. The solid line represents the result of a viscosity measurement on a random poly(ethylene–propylene) copolymer with a similar ethylene propylene ratio as PEP ($\log a_T = 4.35(T - 298)/(T - 175)$).[35] The experimental results agree quite well with the shift factor obtained from viscosity. This disagrees somewhat with our previous results.[24] The difference originates from the explicit consideration of a temperature-dependent segment length, which was neglected in ref 24.

To relate the measured microscopic entanglement distances to the viscoelastic behavior of PEP, the plateau moduli of the large M_w PEP III sample were measured as a function of temperature. Data were obtained over the temperature range $298 \le T \le 548$ K. After every scan at temperatures higher than 448 K, the sample was returned to 448 K and a frequency scan was performed at that temperature to examine possible thermal degradation. This was not found for any specimen and was confirmed by SEC. Attempts were made to acquire data at 573 K, but the sample was found to undergo slight thermal degradation as indicated by the subsequent frequency scan at 448 K (decrease in η_0 and G_m'') and SEC analysis.

Because of the narrow molecular weight distribution of the samples used, G'' possesses a maximum G_m'', occurring at a frequency ω_m. G_m'' can be related to the plateau modulus G_N° according to ref 36, $G_n^\circ = 3.56G_N^\circ$. The G_m'' values were obtained by an interpolation procedure: the data near G_m'' (usually 8–10 data points) were fit by a fifth-order polynomial, and the resulting polynomial was used to determine the maximum in the G'' curve.

Figure 10 shows the temperature dependence of G_m'' for two different PEP III samples. The sample represented by the solid points was run in an effort to define more completely the high-temperature region, which shows an apparent plateau above 200–225 °C. The $G_m''(T)$ values for each sample were normalized using the respective values of G_m'' obtained at 175 °C for each sample. Table VI summarizes the values used to generate Figure 10. The small differences in absolute magnitude of G_m'' (175) between the two samples (<5%) are consistent with slight calibration changes and sample loading differences.

5. Discussion

5.1. Density and Temperature Dependence of the Entanglement Distance. The origin of entanglement constraints so far has been approached on the basis of geometrical or topological considerations relating to the nature of polymers being long flexible and uncrossable objects. As discussed in section 2, two length parameters are of importance: (i) the interchain distance, which is related to the contour length density L/V, and (ii) the step length of the random walk of the chain given by the Kuhn length l_K. To experimentally access the different theories, we systematically varied both lengths. On PEB-2 we studied the dependence on contour length density by varying the polymer volume fraction ϕ at constant temperature over a wide concentration range ($0.25 \le \phi \le$

Table V
Microscopic Parameters for Alternating Poly(ethylene-propylene) and Temperature-Independent Invariants of the Various Scaling Models Calculated for the Case of PEP

T (K)	d (Å)	Wl^4 (10^{-13} Å^4 s^{-1})	$C_\infty(T)$	$\rho(T)$	$d\rho^{1/2}$	$d\rho C_\infty$	$d\rho^{0.61}C_\infty^{0.21}$	$dC_2^{1/3}\rho^{2/3}$	$d^2G_N^\circ/(\rho TC_\infty)$
373	35.2 ± 2.2	0.236 ± 0.022	6.54	0.810	31.7	186	46.8	56.9	0.68 ± 0.09
423	40.0 ± 0.9	0.95 ± 0.07	6.21	0.782	35.4	194	51.5	62.1	0.79 ● 0.04
457	43.0 ± 0.7	1.65 ± 0.1	6.09	0.764	37.6	200	54.3	65.3	0.86 ± 0.03
492	47.5 ± 0.4	3.26 ± 0.11	5.98	0.745	41.0	212	58.8	70.6	0.98 ± 0.02
523	51.3 ± 0.5	4.30 ± 0.16	5.89	0.729	43.8	220	62.5	74.8	1.11 ± 0.02
548	49.9 ± 0.8	3.68 ± 0.37	5.84	0.717	42.3	209	60.1	71.7	1.02 ± 0.03
573	51.7 ± 0.9	4.65 ± 0.99	5.80	0.704	43.4	211	61.4	73.3	1.06 ± 0.03
598	49.5 ± 0.8	5.30 ± 0.93	5.77	0.692	41.2	198	58.1	69.2	0.96 ± 0.03

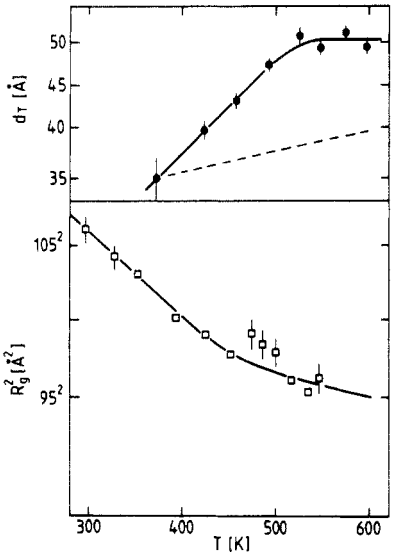

Figure 8. Entanglement distance d and radius of gyration R_g[2,34] for PEP as a function of temperature. The solid lines are guides for the eye. The dashed line in the upper part presents the scaling prediction (see text).

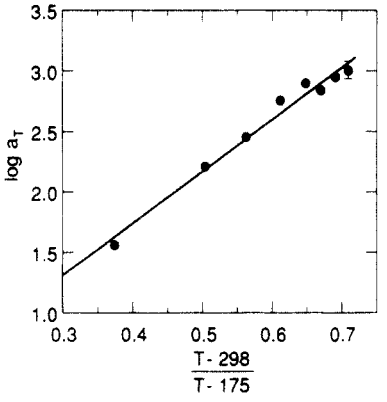

Figure 9. Temperature dependence of the monomeric friction coefficient of PEP in terms of a_T, the shift factor. The solid line displays a viscosity result from a random ethylene–propylene copolymer with similar ethylene–propylene content (56:42).[35]

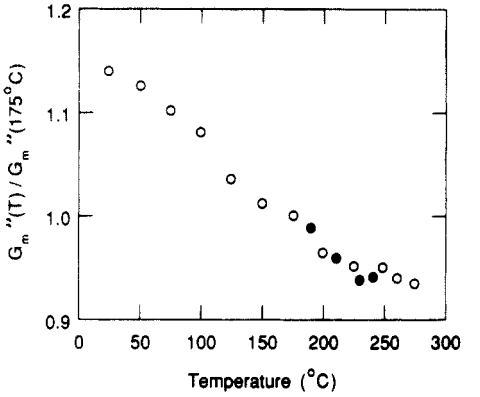

Figure 10. Temperature dependence of $G_m''(T)/G_m''$ (175 °C), being proportional to the plateau modulus $G_N^\circ(T)$. The different symbols signify two different samples.

Table VI
PEP III G_m'' Values Used To Generate Figure 10 (All Values Interpolated Using a Polynomial Fit)

T (°C)	G_m'' × 10^{-6} (dyn/cm^2)	w_{max} (rad/s)
	First Sample	
25.1	3.064	1.229×10^{-2}
50.5	3.022	7.286×10^{-2}
75.3	2.958	0.2754
99.6	2.902	0.8203
125.3	2.781	1.970
150.1	2.720	3.913
175.5	2.687	6.926
199.9	2.587	11.47
225.0	2.548	17.62
249.6	2.550	25.76
259.5	2.518	31.01
274.6	2.511	37.50
299.7	2.426[a]	59.57
	Second Sample	
174.6	2.802	7.211
175.1	2.827	7.031
189.9	2.780	9.705
210.1	2.694	13.82
229.5	2.637	18.92
240.3	2.644	22.18

[a] Found via SEC to be influenced by a small degree of chain degradation.

1). The dependence on l_K was investigated by changing temperature and thereby C_∞ at a given ϕ. For PEP only temperature-dependent measurements were carried out. Other than the dependence on volume fraction, which at least in the concentrated regime can be studied without changing other chain parameters, the temperature-dependent experiments have the inherent disadvantage that, besides a change of l_K, density changes occur, influencing L/V.

We shall now compare the predictions of the various scaling models with the results obtained from PEB-2. For the concentration dependence of the entanglement distance we found $d \sim \phi^{-0.61}$. In terms of the general scaling model of Graessley and Edwards (eq 5)[3] this concentration dependence determines the scaling exponent $a = 2.22 \pm 0.04$. This exponent lies between the predictions of the binary contact model, requiring a fixed number of binary contacts along an entanglement strand ($a = 2$),[6,7] and the Colby–Rubinstein modification,[18] asking for a fixed number of binary contacts within an entanglement volume ($a = {}^7/_3$). The packing model ($a = 3$ or $d \sim \phi^{-1}$) is clearly excluded. Our result also agrees with recent viscoelastic results on polybutadiene solutions—PB is the mother polymer of PEB-2—resulting in a slightly larger value of $a = 2.3$.[37]

Having determined the scaling exponent a, we now may examine the scaling prediction with respect to l_K or C_∞,

respectively. The temperature dependence of C_∞ for PE has recently been studied by Boothroyd et al. by SANS on PEB-2 melts.[31] In a similar T range as our experiments they find d ln C_∞/dT = $-1.15 \pm 0.2 \times 10^{-3}$ K^{-1}. Using d ln ρ/dT = -0.7×10^{-3} K^{-1},[38] eq 5 predicts

$$d^2(T) \approx C_\infty^{-0.44}\rho^{-1.22} \sim \exp[(1.4 \pm 0.1) \times 10^{-3}T] \quad (17)$$

This has to be contrasted with the experimental result of d ln d^2/dT = $2.4 \pm 0.4 \times 10^{-3}$ K^{-1} (eq 16), which is nearly 3 standard deviations larger. To visualize the discrepancy, we have included the theoretical prediction of eq 17 also in Figure 6 as a solid line. Experimental results and scaling predictions are clearly apart.

For PEP we have studied only the temperature dependence of d. Therefore, an independent evaluation of the scaling exponent from the volume fraction dependence is not possible. In Table V we examine the different scaling models in comparing the invariants with respect to temperature of the different models: $d\rho^{1/2}$ for the binary contact model (eq 11); $d\rho C_\infty$ for the packing model (eq 7); $d\rho^{0.61}C_\infty^{0.22}$ for the general scaling model (eq 5), where we took the exponent from PEB; and $dC_\infty^{1/3}\rho^{2/3}$ for the modified binary contact model. In all cases the invariants are far from being constant but increase systematically with temperature—the temperature-dependent increase of the entanglement distance is not compensated by the decrease of C_∞ and ρ. For the prediction of the general scaling model taking a = 2.22 from PEB we have displayed the results in Figure 8. Obviously, the differences are far larger than those for PEB shown in Figure 6.

Earlier viscoelastic experiments on the plateau moduli of various polyolefins and polydienes as a function of microstructure and temperature have shown that the scaling model is capable of accounting at least qualitatively for the observed trends as it concerns the dependence on contour length density—in varying the microstructure—and temperature.[32] Our results demonstrate that on a qualitative level there is also a broad agreement for PEB, while for PEP larger discrepancies appear to emerge. Quantitatively, our observations on PEB disagree outside the errors of the experiment.

Concerning the topological model of Iwata and Edwards,[9] which other than conjecturing on the basis of scaling arguments actually calculates entanglement constraints on a geometrical basis, a direct quantitative comparison would require extensive calculations using the molecular parameters of the two polymers. These calculations have not been made, leaving us with a qualitative comparison. The model predicts $G_N^\circ \approx \phi^a$, with $1.97 \leq a \leq 2.2$ enveloping our value of a = 2.22 ± 0.04. However, at high contour length density, as realized in PEB-2, the exponent would be expected more close to a = 2. The topological interaction parameter γ, measuring the capability of a chain to entangle, is predicted to be a monotonously increasing function of C_∞ or the entanglement distance d should monotonously decrease with increasing C_∞. On a qualitative level for both polymers we observe such a behavior. To quantify for PEB-2: if we assume that the density dependence would be correctly described by the scaling model $d^2 \approx \rho^{1-a}$, then $d^2 \approx C_\infty^{-1.4}$ is found.

5.2. On the Relation of Tube Diameter and Plateau Modulus. The reptation theory of viscoelasticity by Doi and Edwards[11,12] relates the plateau modulus G_N° to the tube diameter d by eq 1. To investigate this relation for PEP we have independently determined the temperature dependence of all quantities appearing in eq 1.

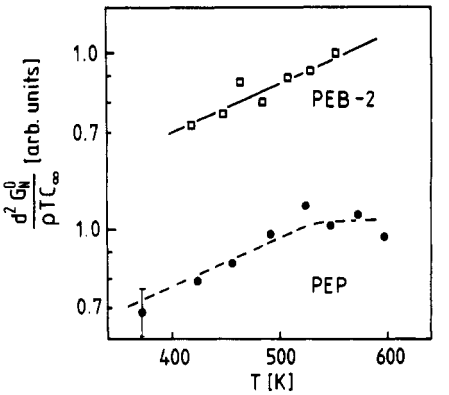

Figure 11. Invariant of eq 1 for PEP and PEB-2 as a function of temperature.

The experiments on $G_N^\circ(T)$ and $d(T)$ are described in section 3, $C_\infty(T)$ have been studied by SANS in a melt over a wide temperature range,[34] and, finally, the temperature dependence of density was measured by Walsh.[39] For PEB we may use viscoelastic data by Carella et al.[32] on a hydrogenated polybutadiene of similar microstructure yielding a plateau modulus essentially independent of temperature. Our rheological measurements support this finding. The temperature-dependent characteristic ratio has been obtained by Boothroyd et al.,[31] while the density temperature coefficient originates from ref 38. With these quantities we may calculate the invariants $d^2G_N^\circ/C_\infty\rho T$, which according to eq 1 should be independent of temperature. The results for PEP are given in Table V, and those for PEB are given in Table III. Figure 11 displays the results: Both polymers exhibit a very similar general behavior. Instead of being constant the "invariant" increases by about 30% over the investigated temperature range. The temperature slopes d ln $[d^2G_N/(\rho TC_\infty)]$/d$T$ $\approx 2.2 \times 10^{-3}$ K^{-1}, thereby, are about equal for both polymers. If we consider that the individual temperature dependence of d and G_N° is quite different for PEP and PEB-2—for PEP G_N° decreases and d increases strongly with T, while for PEB-2 G_N° is practically constant[32] and d increases only weakly—the nearly identical temperature dependence of the invariant is remarkable. It demonstrates that the Doi–Edwards relation between plateau modulus and tube diameter or, more generally, the rubber analogue connecting temporary mesh and modulus is only approximately valid. The extra temperature dependence indicates the existence of some additional dynamic contributions to G_N° and d which are not taken into account in purely geometrical models.

6. Conclusion

We presented NSE experiments on the dynamic structure factor from PEB-2 and PEP melts for different temperatures; for PEB-2 also the effect of dilution with an oligomer was investigated. The experiments were designed to answer questions about the molecular origin of entanglements. For this purpose we varied the temperature and the polymer volume fraction. Thereby, we studied the dependence of the entanglement distance on the two length parameters considered to be important for the formation of entanglements. Changing the polymer volume fraction (PEB), we altered the interchain distance and thus the contour length density. The obtained scaling exponent a = 2.22 ± 0.04 excludes the packing model and lies between the binary contact model demanding a fixed number of binary contacts/entanglement strand (a = 2) and that asking for a fixed number of contacts/entanglement volume (a = $^7/_3$). Varying the temperature, we

changed the step length of the random walk of a chain for PEB-2 and PEP. The scaling model is not able to describe the dependencies on volume fraction and flexibility simultaneously. Qualitatively, our results agree with the topological calculations by Iwata and Edwards.[9] However, a quantitative comparison still has to be done. The interpretation of the plateau modulus as a temporary rubber relates molecular chain parameters, entanglement distance, and plateau modulus. An independent measurement of all quantities involved facilitates a test of the prediction of the Doi–Edwards theory. For PEB-2 and PEP systematic deviations are found, implying that the plateau modulus decreases more weakly than required by the increase of the entanglement distance. The fact that both polymers exhibit very similar deviations may indicate the presence of a further dynamic mechanism beyond the purely geometrical interaction.

References and Notes

(1) Ferry, J. D. *Viscoelastic Properties of Polymers*; Wiley: New York, 1980.
(2) Doi, M.; Edwards, S. F. *The Theory of Polymer Dynamics*; Clarendon: Oxford, 1986.
(3) Graessley, W. W.; Edwards, S. F. *Polymer* **1981**, *22*, 1329.
(4) Kavassalis, T.; Noolandi, J. *Macromolecules* **1988**, *21*, 2869.
(5) Colby, R. H.; Rubinstein, M. *Macromolecules* **1990**, *23*, 2753.
(6) Edwards, S. F. *Proc. Phys. Soc.* **1967**, *92*, 9.
(7) De Gennes, P.-G. *J. Phys. Lett.* **1974**, *35*, L-133.
(8) Edwards, S. F. *Proc. R. Soc. London, A* **1988**, *419*, 221.
(9) Iwata, K.; Edwards, S. F. *J. Chem. Phys.* **1989**, *90*, 4567.
(10) De Gennes, P.-G. *J. Chem. Phys.* **1971**, *55*, 572.
(11) Doi, M.; Edwards, S. F. *J. Chem. Soc., Faraday Trans. 2* **1978**, *74*, 1789; **1978**, *74*, 1802; **1978**, *75*, 38.
(12) Graessley, W. W. *Adv. Polym. Sci.* **1974**, *16*, 1.
(13) Klein, I. *Nature* **1978**, *271*, 143.
(14) Richter, D.; Farago, B.; Fetters, L. J.; Huang, J. S.; Ewen, B.; Lartigue, C. *Phys. Rev. Lett.* **1990**, *64*, 1389.
(15) Richter, D.; Butera, R.; Fetters, L. J.; Huang, J. S.; Farago, B.; Ewen, B. *Macromolecules* **1992**, *25*, 6156.
(16) Ronca, G. *J. Chem. Phys.* **1983**, *79*, 1031.
(17) Lin, Y. H. *Macromolecules* **1987**, *20*, 3080.
(18) Colby, R. H.; Rubenstein, M.; Viovy, J. L. *Macromolecules*, in press.
(19) Doi, M. *J. Phys. A* **1975**, *8*, 959.
(20) Wu, S. *J. Polym. Sci.* **1989**, *27*, 723.
(21) Aharoni, S. M. *Macromolecules* **1983**, *16*, 1722.
(22) Rachapudy, H.; Smith, G. G.; Raju, V. R.; Graessley, W. W. *J. Polym. Sci., Polym. Phys. Ed.* **1979**, *17*, 1211.
(23) See, e.g.; Mezei, F. In *Lecture Notes in Physics*; Mezei, F., Ed.; Springer-Verlag: Berlin, Heidelberg, New York, 1980; Vol. 128.
(24) Butera, R.; Fetters, L. J.; Huang, J. S.; Richter, D.; Pyckhout-Hintzen, W.; Zirkel, A.; Farago, B.; Ewen, B. *Phys. Rev. Lett.* **1991**, *66*, 2088.
(25) Richter, D.; Ewen, B.; Farago, B.; Wagner, T. *Phys. Rev. Lett.* **1989**, *62*, 2140.
(26) Higgins, J. S.; Fruitwalu, H.; Tomlins, P. E.; Clark, J. N. In *Springer Proceedings in Physics*; Richter, D., Springer, T., Eds.; Springer-Verlag: Berlin, Heidelberg, New York, 1988; Vol. 29.
(27) Rouse, P. E. *J. Chem. Phys.* **1953**, *21*, 1273.
(28) De Gennes, P.-G. *Physics (Long Island City, N.Y.)* **1967**, *3*, 37.
(29) Oeser, R.; Ewen, B.; Richter, D.; Farago, B. *Phys. Rev. Lett.* **1988**, *60*, 1041.
(30) De Gennes, P.-G. *J. Phys. (Paris)* **1981**, *42*, 735.
(31) Boothroyd, A. T.; Rennie, A. R.; Boothroyd, C. B. *Europhys. Lett.* **1991**, *15*, 715.
(32) Carella, J. M.; Graessley, W. W.; Fetters, L. J. *Macromolecules* **1984**, *17*, 2775.
(33) As has been discussed in ref 15, deviations between the Ronca model and the experimental results are evident if the experiment is carried to observation times considerably larger than the crossover time between unrestricted Rouse and local reptation behavior. This is the case for PEB-2. An evaluation in terms of local reptation, on the other hand, requires one to disregard the data taken at times shorter than this crossover time. For PEP such a procedure would necessarily have to disregard a large part of the measured spectra.[15] Therefore the Ronca model was used for data evaluation. As has been demonstrated for PEB-2, the resulting values for d are only marginally different.
(34) Zirkel, A.; Richter, D.; Pyckhout-Hintzen, W.; Fetters, L. J. *Macromolecules* **1992**, *25*, 954.
(35) Richards, J. R.; Maneke, R. G.; Ferry, J. D. *J. Polym. Sci., Polym. Lett. Ed.* **1964**, *2*, 197.
(36) Raju, V. R.; Menezes, E. V.; Marin, G.; Graessley, W. W.; Fetters, L. J. *Macromolecules* **1981**, *14*, 1668.
(37) Colby, R. W.; Fetters, L. J.; Funk, W. G.; Graessley, W. W. *Macromolecules* **1991**, *24*, 3873.
(38) Christ, B.; Tanzer, J. D.; Graessley, W. W. *J. Polym. Sci., Polym. Phys. Ed.* **1987**, *25*, 545.
(39) Walsh, D., private communication ($d \ln \rho/dT = -0.697 \times 10^{-3}$ K^{-1}).